New insights on metals in the Arctic aerosol in a climate changing world

Silvia Becagli[1], Laura Caiazzo[1,2], Tatiana Di Iorio[3], Alcide di Sarra[3], Daniela Meloni[3], Giovanni Muscari[4], Giandomenico Pace[3], Mirko Severi[1], Rita Traversi[1].

[1] Department of Chemistry, University of Florence, Sesto Fiorentino, 50019 Florence, Italy

[2] Istituto Nazionale di Fisica Nucleare INFN sez. Firenze, Sesto F.no, 50019 Florence, Italy

[3] ENEA, Laboratory for Observations and Analyses of Earth and Climate, 00123 Rome, Italy

[4] Istituto Nazionale di Geofisica e Vulcanologia, INGV, Rome, 00143, Italy

***Keywords**: Metals, Arctic, Greenland, Aerosol, PM_{10}, Thule.*

Abstract.

Ship traffic, population, infrastructure development, and mining activities are expected to increase in the Arctic due to its rising temperatures. This is expected to produce a major impact on aerosol composition. Metals contained in atmospheric particles are powerful markers and can be extremely helpful to gain insights on the different aerosol sources. This work aims at studying the sources of metals in the Arctic aerosol sampled at the Thule High Arctic Atmospheric Observatory (THAAO; Greenland, 76.5°N 68.8°W).

Due to the particular composition of Greenlandic soils and to properties of other sources, it was possible to find several signatures of natural and anthropogenic aerosols transported from local and long-range regions.

Arctic haze (AH) at Thule builds up on long-range transported aerosol mainly from Canada and Nord America. From a chemical standpoint, this aerosol is characterized by a high concentration of sulfate, Pb, As

and Cd and by a La/Ce ratio larger than 1. The Ti/Al and Fe/Al ratios in the AH aerosol are lower (Ti/Al= 0.04 w/w; Fe/Al=0.79 w/w) than for local aerosol (Ti/Al= 0.07 w/w; Fe/Al=0.89 w/w).

Conversely, aerosol arising from coastal areas of South-West Greenland is characterized by a high concentration of V, Ni, and Cr. These metals, generally considered anthropogenic, arise here mainly from natural crustal sources. In some summer samples, however, the V/Ni ratio becomes larger than 3. In particular, cases displaying this characteristic ratio, as also shown by backward trajectories, are associated with sporadic transport to Thule of ship aerosol from ships passing through Baffin Bay and arriving to Thule during summer.

Although further measurements are necessary to confirm the discussed results, the analysis carried out in this work on a large number of metals sampled in coastal Greenland aerosol is unprecedented.

1. Introduction

It is now demonstrated that climate change is amplified in the Arctic region. Arctic amplification has been found in past warm (Barron, 1983) and glacial periods (Dahl-Jensen et al., 1998), as well as in historical observations (Chapman and Walsh, 1993; Bekryaev et al., 2010) and climate model experiments (Holland and Bitz, 2003, Pithan and Mauritsen, 2014).

The Arctic lower troposphere is influenced by pollution from local and high-latitude Eurasia and North America sources, the latter being currently poorly quantified. These sources include emissions associated with resource extraction (e.g., flaring of gas associated with oil production; Stohl et al., 2013) and shipping (e.g., Corbett et al., 2010; Aliabadi et al., 2015). Such local sources are already influencing atmospheric composition on local and regional scales (Law et al., 2017, and reference therein).

One of the results of climate change in the Arctic is the sea ice loss that may increase accessibility of the Arctic. It is expected that new shipping routes within the Arctic Ocean will seasonally open up, substantially decreasing transport distances between Asia, North America, and Europe. This may result in up to 5% of global shipping traffic moving to high Arctic routes (Corbett et al., 2010). In addition, a large portion of the Earth's undiscovered oil and gas is predicted to be under the Arctic Ocean floor and will be increasingly

exploited in the future (Peters et al., 2011; Gautier et al., 2009). Population, urbanization, infrastructure development, and mining activities are also expected to increase in the Arctic (Andrew, 2014), adding to local emissions of air pollutants, unless compensated by tighter pollutant emission controls. A detectable increase in particulate matter concentrations at Resolute Bay, on remote Lord Cornwallis Island, in Canada, has been associated with ship traffic in the newly accessible Northwest Passage (Aliabadi et al., 2015). Similar increases have been associated with cruise ship traffic near Svalbard in the Norwegian Arctic (Eckhardt et al., 2013).

In this environmental changing ecosystem, it is crucial to improve quantification of the relative contributions of different anthropogenic pollutant sources to provide a rigorous scientific basis for sustainable solutions and adaptive strategies.

Metals are powerful markers for source identification but their concentration in Arctic aerosol is quite low, therefore requiring high performance analytical techniques (Giardi et al., 2018) or low temporal resolutions (Conca 2019, Gong and Barry, 2005). For this reason, information on metals as tracers of aerosol sources in the Arctic aerosol are scarce.

In this work, we describe an improved easy-to-use high sensitive analytical method for metal quantification in the Arctic aerosol through the ICP-AES (Inductively Coupled Plasma – Atomic Emission Spectroscopy) technique, coupled with a desolvation inlet system to increase the analytical performance of the technique. This analytical method has been used to analyze about two years (2016-2017) of Arctic samples allowing the determination of 15 elements at relatively high temporal resolution. This analysis leads to obtain unique information on metal concentration, variability and sources. In addition, the dataset reveals some characteristic ratios, which appear as very promising tools for the definition of a fingerprint of aerosol sources in such a crucial region of the Earth.

2. Methodology

2.1 Sampling site and aerosol collection

PM_{10} aerosol sampling is performed at the Thule High Arctic Atmospheric Observatory (THAAO;

http://www.thuleatmos-it.it) at Thule Air Base (76.5°N 68.8 °W, hereafter indicated simply as Thule), Greenland (Fig.1). THAAO is located on South Mountain at 220 m elevation a.s.l., at a 20-minute drive from main base. Various ground-based instruments installed at the observatory are part of the international Network for Detection of Atmospheric Composition Change (NDACC, http://www.ndsc.ncep.noaa.gov). The station is a few kilometers away from the nearest village and it is not influenced by local emissions, thanks to the wind main directions (Muscari et al., 2014). The aerosol sampling activity started in 2010 and is carried out all year round at 48 h resolution. Here we show about 2 years of aerosol chemical data from December 2015 to October 2017. Some interruptions in the sampling occurred due to technical problems.

Aerosol sampling is performed by using a TECORA Skypost sequential sampler, equipped with a PM_{10} sampling head, operating in accord with the EN 12341 European rules (air flow: 2.3 m^3/h; actual conditions; Becagli et al., 2016).

Aerosol samples are collected on Teflon (PALL Gelman) filters, 47 mm in diameter, with 2.0 µm nominal porosity but with 99.5% sampling efficiency for 0.3 µm aerodynamic diameter particles. Filters are weighted in Italy before shipment to THAAO. After sampling filters are kept in their plastic Petri dish and shipped to Italy. They are kept frozen until they are weighted, cut, extracted and analyzed.

The PM_{10} mass is determined by the difference of the filters weight before and after the sampling. The weighting was performed on a 5-digit microbalance (Sartorius analytical balance) equipped with ionic cannon to avoid error weighting due to the electrostatic charge of the filters. Before the weighting, the filters were stored in a dryer for 48 h, with 50±5% relative humidity. After weighting, each filter was cut exactly in two halves, one devoted to the ions determination and the other to the metal determination.

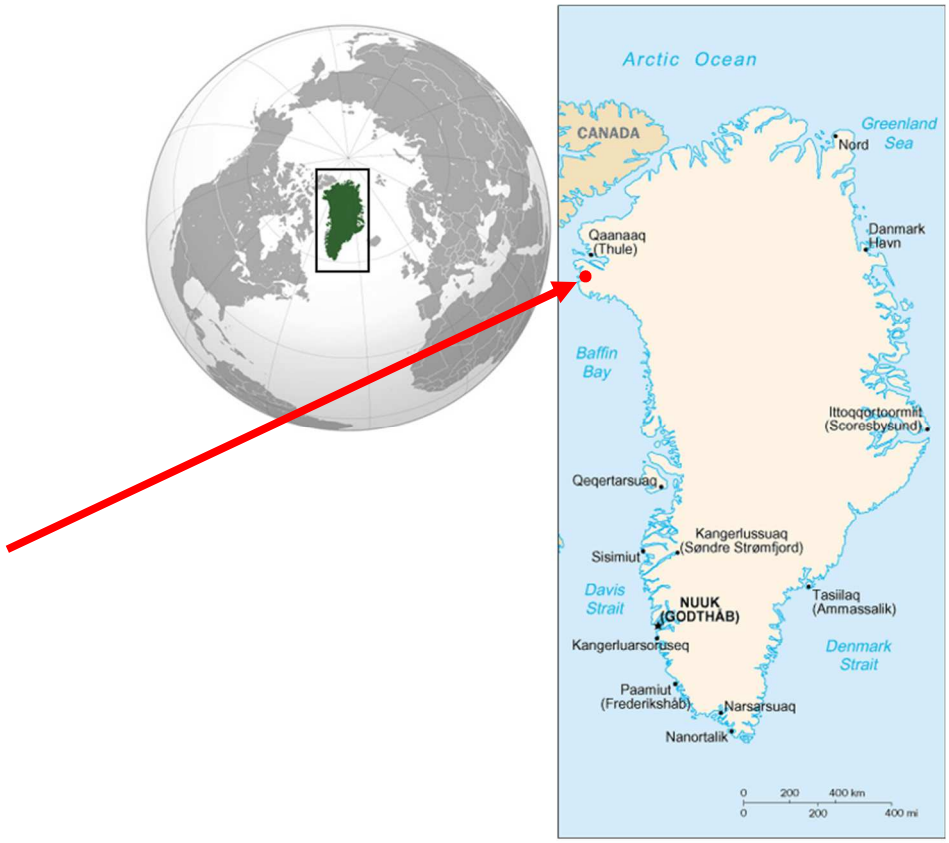

Figure 1. Map of the Greenland with the sampling site (indicate by the red arrow) and other places reported in the text.

2.2 Chemical analysis

The half filter devoted to the ions determination is extracted in ultra pure water (R > 18 MΩ·cm) and analyzed by ion chromatography (IC), allowing the determination of important ionic markers on the same sample. Details on the IC measurements are reported in Becagli et al. (2016). The detection limit (DL) were 0.1 µg/L corresponding to 0.02 ng/m^3 atmospheric concentration for most ions in these sampling (48 h resolution, i.e. 110 m^3 of sampled air) and analytical (half filter extracted in about 10 mL of ultrapure water) conditions, excluding NH_4^+ and low molecular weight carboxylic anions for which the DL is 1 µg/L, corresponding to 0.2 ng/m^3.

The low concentration of metals in aerosol samples requires specific attention to the cleaning in every step of the process. Solutions are prepared using ultrapure water (R > 18 MΩ·cm) obtained from a Millipore purification system (Massachusetts, USA). All acid solutions are prepared from concentrated HNO_3 sub-

boiled distilled (s.b. HNO_3), starting from 65% nitric acid for analysis.

In order to avoid contamination, all filter-handling operations are accomplished by wearing powder-free gloves, working under a Class 100 laminar flow hood. Previous tests demonstrated that polyethylene ring has a not negligible metal content, especially for Al, Zn, and Cu when compared to the Arctic aerosol concentration (Giardi et al., 2018). Therefore, before the solubilization procedure, the polyethylene ring of each half filter devoted to metal determination is removed by using a stainless steel blade.

The solubilization procedure for metal determination is performed with a microwave oven (Mars Xpress, CEM, Italy) following the European rule UNI EN 19402 protocol and is reported in detail by Giardi et al. (2018). Briefly, each half filter is added to 2 mL of s.b. HNO_3 and 0.5 mL of 30% H_2O_2 (Merk Suprapure grade) in Teflon-PFA vessels. The digestion program in the microwave oven is arranged in three different steps: 20 min to increase temperature up to 220 °C and pressure to 30 atm; stable values of temperature and pressure for 25 min; cool down to room temperature for 20 min.

The final solution volume is about 10 mL, coming from at least 3 consecutive rinses of the vessel with 1% HNO_3 in ultrapure water. The exact volume is determined gravimetrically.

After each mineralization, the vessels are cleaned with the same microwave oven program by using about 1 mL of s.b. HNO_3 and 1 mL of ultrapure water.

For metals determination the calibration procedure with Ge as internal standard is used. Samples and calibration standards signals are normalized with respect to the signal of Germanium at concentration of 1 ppm.

Exactly 5 mL of the sample are transferred into clean disposable polyethylene tubes and spiked with 0.1 mL of Ge 50 ppm just before analysis. A 100 ppm multi standard is used for the calibration curves.

The metals are determined by using a 720-ES ICP – AES (Varian, Palo Alto, California) equipped with auto sampler and Ultrasonic Nebulizer (CETAC, Nebraska, USA). The ultrasonic nebulizer is preferred to the spray chamber, as it produces a thinner and more homogeneous spray increasing sensitivity, producing a up to 10 times smaller detection limit (Rugi et al., 2015). The detection limit (DL), for each element is reported in Table 1.

Table 1. Detection limit (DL) and reproducibility for metals determination by ICP-AES. The DL is calculated as the concentration corresponding to the signal = 3σ, where σ is the standard deviation of 10 measurements of the standard at 1 μg/L. The DL in the atmosphere are calculated considering that we use ½ filter, 10 mL of solubilization volume, and 110 m^3 of sampled air (corresponding to 48 h of sampling at 38.3 L/min as reported in EU rules). λ_{meas} is the emission wavelength used for the quantification of each metal. * data from Giardi et al. (2015) using the same solubilization procedures. ^ data from Conca et al. (2015) using the same solubilization procedures. $^{\$}$ data from Zhan et al., 2014 by using a slightly different solubilization procedure (HNO_3 in Microwave oven). $^{@}$ Unpublished data, see text for explanation.

Metals	λ_{meas}	**DL (solution) μg/L**	**DL (atmosphere) ng/m³**	**Reproducibility at 2 μg/L %**	**Reproducibility at 10 μg/L %**	**Recovery %**
Al	396.152	0.240	0.044	2.6	2.6	91-104$^{\$}$ 71-96 $^{@}$
As	188.980	0.200	0.036	7.8	2.5	>80^ 91-104$^{\$}$
Ba	233.527	0.050	0.009	1.0	2.2	91-104$^{\$}$
Cd	214.439	0.010	0.002	1.9	2.1	>80^ 91-104$^{\$}$
Ce	418.659	0.130	0.024	3.3	2.5	85 * >80^
Cr	267.716	0.050	0.009	1.0	2.1	91-104$^{\$}$
Fe	238.204	0.130	0.024	1.8	2.5	>80^ 91-104$^{\$}$

La	333.749	0.020	0.004	1.0	2.0	87*
Mn	257.610	0.090	0.016	1.4	2.1	>80^ 91-104$
Ni	231.618	0.100	0.018	1.5	2.1	>80^ 91-104$
Pb	220.353	0.220	0.040	3.2	2.4	>80^ 91-104$
Si	250.690	2.540	0.462	1.3	2.0	<30@
Ti	334.941	0.060	0.011	1.0	2.1	17-54@
V	292.401	0.040	0.007	1.0	2.0	>80^ 91-104$
Zn	202.548	0.370	0.067	1.8	2.3	>80^ 91-104$

The detection limits obtained by means of this analytical method using ICP-AES are larger than those obtained by ICP-MS by Giardi et al. (2018) and Conca et al. (2019). On the other hand, ICP-AES is easier to manage than the HR-ICP-MS and by reducing the levels of fields blank and by sampling about 110 m^3 of air (48h resolution), these values of DL allow us to reliably determine the metals reported in table 1 in most samples.

A detailed study of blanks for each element was accomplished in order to determine the blanks level. Procedural blanks (including digestion tubes, laboratory handling operations and reagents) and reagents blanks (ultrapure water, sub-boiled HNO_3, and suprapur hydrogen peroxide) reveal that the most relevant source of contamination is the whole set up of operations carried out in the extraction protocol. Despite the very low blank values we find, they are not negligible because of the very low concentration of the analyzed metals. Therefore, if the blank values was lower than the mean values in real samples by one order of magnitude then the blank value of each element in each extraction procedure was subtracted

from the concentration in the sample and the datum was retained in the subsequent analysis. Otherwise, the metal determination was not considered reliable and was not used in the analysis when the blank was > 0.1 times the mean concentration.

The recovery for each reliability determined element is also reported in table 1. These recoveries were reported for La and Ce in Giardi et al. (2015) and for As, Cd, Ce, Fe, Mn, Ni, Pb, V, Zn in Conca et al. (2019) by using the same solubilization procedure here used on certified material Amis 0356REEL Carbonatite Wigu TZ (Amis Republique of South Africa) and NIST 1648a "urban particulate matter" respectively. For Al, As, Ba, Cd, Fe, Mn, Ni, Pb, V and Zn, Zhan et al. (2014) reports a recovery in the range 91-104% by using a slightly different digestion procedure (only HNO_3 and lower temperature in microwave oven). It is known that Si and Ti are present in mineral having scarce solubility in HNO_3 or HNO_3-H_2O_2 also at high temperature, besides their solubility is site and size dependent. Indeed, by comparing concentration data on Al, Si, and Ti obtained on the HNO_3-H_2O_2 extraction procedure and the total content obtained by particles induced X ray emission (PIXE) in sites having different anthropic and dust impacts in the Mediterranean region we find the recovery reported in table 1 for these elements (unpublished data).

2.3 Non-sea salt sulphate calculation

SO_4^{2-}originates from multiple sources. In order to exclude the contribution of sea spray, the non-sea salt (nss) SO_4^{2-} fractions were calculated as follows:

$nssSO_4^{2-} = SO_4^{2-} - (SO_4^{2-}/Na^+)_{sw} * Na^+$,

where SO_4^{2-} and Na^+ are the ions analytical concentrations determined by IC, and $(SO_4^{2-}/Na^+)_{sw} = 0.25$ is the mean ratio of the ions in the seawater (Henderson and Henderson, 2009).

2.4 Enrichment factor calculation

The enrichment factor (EF) with respect to the crustal source, for a specific element X, is calculated by using Al as marker for crustal aerosol. Al is chosen as crustal marker instead of Si because of the relatively large uncertainty on Si recovery in the digestion procedure used here.

189 The following equation is used for EF calculation:

190 $EF_X=(X/Al)_{sample}/(X/Al)_{ucc}$

191 where $(X/Al)_{sample}$ is the ratio between metal X and Al concentrations in the sample, and $(X/Al)_{ucc}$ is the same
192 ratio in the upper continental crust (UCC). $(X/Al)_{ucc}$ is given by Henderson and Henderson (2009).

193 EF values in the range 1-10 are typical of elements having crustal source, EF values higher than 10 indicate
194 the presence of non crustal sources.

195 **2.5. Backward trajectory calculation**

196 Airmass backward trajectories were generated by the Hybrid Single-Particle Lagrangian Integrated
197 Trajectory (HYSPLIT) model (Stein et al., 2015) using the NCEP Reanalysis meteorological database and the
198 model vertical velocity. Trajectories arriving at Thule at 200 m a.g.l. were computed.

199 **3. Results and discussion**

200 **3.1 Concentration range and enrichment factors with respect to the upper continental crust**

201 Figure 2a reports the box plots of concentrations measured for each metal by ICP-AES. The median and
202 mean values are generally in the concentration range of those reported by Shevchenko et al. (2003) at
203 several sites in the Russian Arctic and by Gong and Barry (2005) at Alert, but are usually larger than
204 concentrations measured at Ny Alesund (Svalbard Islands) by Conca et al. (2019).
205 Al, Fe, Si, and Zn show the highest concentrations among the measured metals (as average 17.0, 17.1, 26.4,
206 15.5 ng/m^3, respectively). It is well known that these metals, excluding Zn, arise by crustal input; indeed,
207 there is a significant correlation among them (figure 1S), and the enrichment factors with respect to Al are
208 close to 1 (figure 2b). Ti, Mn, and Ba display the lowest mean concentrations (1.0, 0.28, 0.18 ng/m^3
209 respectively) among the crustal elements, ranging from the DL up to maximum values of 7.5, 2.0, 0.87
210 ng/m^3 respectively. Data suggest that also for these elements the crustal source is dominant, due to the
211 significant correlation with Al (figure 1S) and the enrichment factors close to 1.

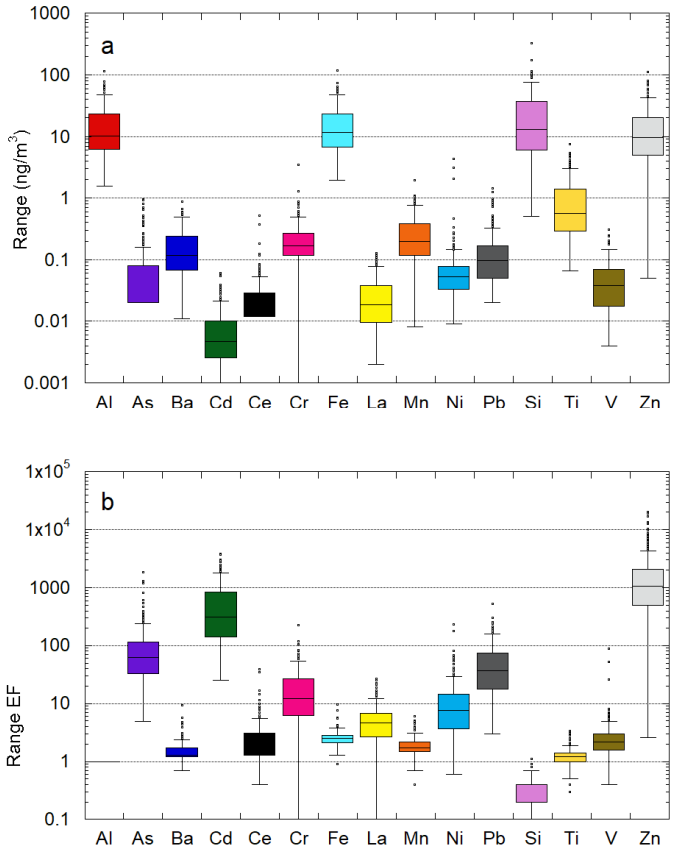

212

213 **Figure 2**. Box plot of elements concentrations (plot a) and EF (plot b). Each box encloses 50% of the data
214 with the median value of the variable displayed as a line. The top and bottom of the box mark the limits of
215 ± 25% of the variable population. Vertical lines over and above the box represent the 1.5 time the
216 interquartile distance. Values out of this range are plotted as single points.

217

218 The pattern of Fe and Ti is particularly interesting: both display a significant linear correlation with Al, with
219 slopes (Fe/Al = 0.88 w/w and Ti/Al = 0.060 w/w) larger than that for UCC (0.43 w/w and 0.047 w/w,
220 respectively; Handerson and Henderson, 2009). Besides, considering that recovery for Ti is not 100%, the
221 Ti/Al ratio in the aerosol samples is underestimated by a factor from 2 to about 5, implying a Ti/Al ratio
222 between 0.12 and 0.30. This suggests a crustal source affecting Thule aerosols enriched in Fe and especially
223 Ti with respect to the average crust. In the proximity of Thule, the presence of highest-grade Ilmenite

mineral ($FeTiO_3$) sand was first identified in 1916 by the Danish and Greenland geological survey after a multi-decade work program run by Denmark (Henriksen et al., 2009). The presence of Ilmenite can justify the large Fe/Al and Ti/Al ratios in the Thule aerosol samples, indicating the prevalence of local dust sources with respect to long-range transported dust.

Contrarily to crustal elements, Pb, As, and Cd show very low concentrations (as average 0.15, 0.086, 0.0079 ng/m^3 respectively) and EF >> 10 (as average 57, 117 and 602 and up to 520, 1865 and 3791 respectively for Pb, As and Cd). Therefore, a strong input from anthropogenic sources is expected for these metals.

V, Ni, and Cr are also expected to have anthropogenic sources; however, their EF values (as average 3.3, 13, 22 respectively) are not so higher than 10 (and lower for V).

La and Ce are the only two REEs determined by ICP-AES as concentrations of REEs are low in crustal material and especially in aerosol samples. Their EFs are close to 1 (figure 2b), and they significantly correlate with Al (figure 1S) as expected due to their dominant crustal source.

3.2 Temporal trend

In this section the time series of each element is reported. Elements are grouped based on their enrichment factors and correlations discussed in section 3.1. In particular, in figure 3a we report the time series of elements having a dominant crustal source (Al, Si, Ti, Mn, Ba), in figure 3b elements having a large anthropogenic source (Pb, As, Cd), in figure 3c elements which usually have an anthropogenic origin but do not show an enrichment with respect to the crust, and in figure 3d the two REEs determined in these samples (La, Ce).

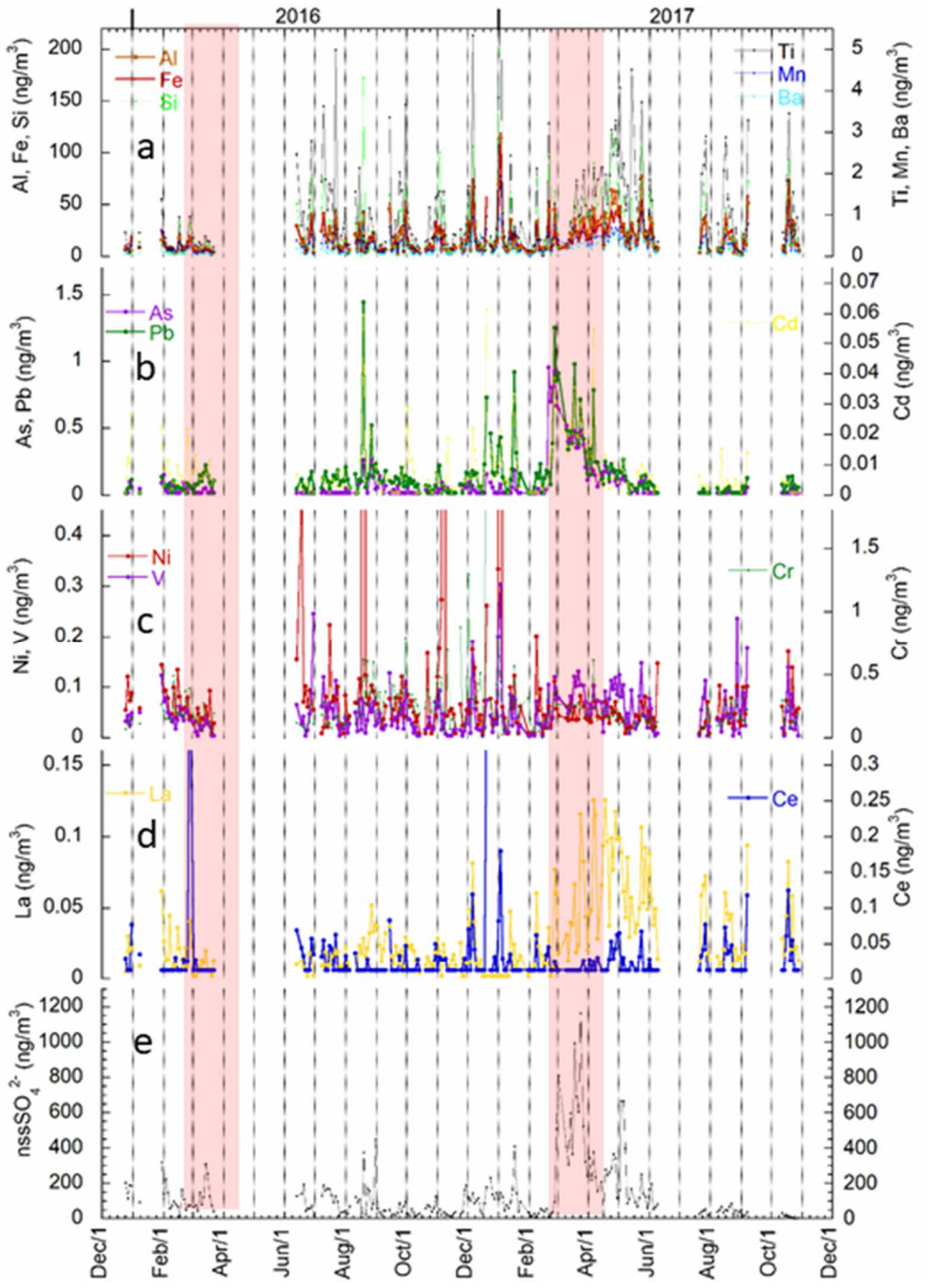

243

244 **Figure 3.** Time series of Al, Fe, Si, Ti, Mn, Ba (plot a), As, Cd, Mn (plot b) , V, Ni, Cr (plot c), La and Ce (plot d)

245 and $nssSO_4^{2-}$ (plot e) in PM_{10} samples at Thule. Shaded areas represent the Arctic Haze period.

246

247 The time series of $nssSO_4^{2-}$ is reported in figure 4e, as it is one of the main constituent of the Arctic Haze

248 (hereafter AH, Quinn et al., 2007).

Crustal markers

Figure 3a shows a general common temporal trend for all the crustal markers, with maximum values in the period between mid-March and May. Interestingly, the period of crustal markers' maximum only partially overlaps the maxima of $nssSO_4^{2-}$ here used as marker of long range transported AH aerosol, suggesting that crustal aerosols may have both long-range and local sources. In order to highlight if the two different sources (Arctic Haze from long-range and local sources) have different characteristic ratio between the crustal markers, two time periods corresponding with different air masses source areas and PM_{10} chemical composition have been chosen: end of February-March 2017, and May 2017. Due to a mixed pattern, April was excluded by the analysis.

In the period end of February-March 2017, that is the time period more impacted by the AH sources (as demonstrated by the highest values of $nssSO_4^{2-}$, see section below) the Ti/Al and Fe/Al ratios present mean values of 0.04 and 0.79 respectively (Figure 2S). In this period the backward trajectory analysis shows that 90% of the air masses arise from Canada and North America, traveling at high altitude (see Figure 3S). A different pattern of backward trajectories is observed in May, with air masses traveling at low altitude over the Greenlandic west coast and in the surrounding of the sampling site (Figure 3S). This more local origin of air masses in May with respect to March affects the Fe/Al and especially the Ti/Al ratios. The latter in May becomes about twice than in March (Ti/Al = 0.07; Fe/Al =0.89). Due to the presence of Ilmenite minerals in the Greenland soil, the Ti/Al and Fe/Al ratios can be considered a fingerprint of local crustal aerosol, allowing to distinguish mineral particles form local and long-range transport from Canada and North America. It has to be remember that due to the incomplete dissolution of Ti this ratio could be still higher (in the range 0.14-0.35).

Anthropogenic markers

High concentration of pollutants are found in the Arctic during the Arctic haze period (see for intance Shaw, 1995; Barrie et al., 1989). The polluted air masses affect the atmosphere over the Arctic Circle and two great lobes that extend down over Eurasia and North America. The rather severe pollution throughout

274 this air masses system in winter is, to a large extent, a result of the lowered rates of particles and gas
275 removal in this cold, dark, and rather stable system. The AH aerosol is composed mainly of sulfate (e.g.
276 Quinn et al., 2007; Barrie et al., 1989) showing a typical seasonal pattern with the highest concentrations
277 occurring roughly from February to April (e.g. Quinn et al., 2007; Shaw, 2005; Barrie et al., 1989).
278 The $nssSO_4^{2-}$ time series (figure 3e) shows the highest concentration in March 2017, then a decreasing
279 trend from April until May. It has to be noticed that in May a certain fraction of $nssSO_4^{2-}$ arises from the
280 oxidation of the biogenic dimethyl sulfide (Becagli et al., 2016). In March 2016, the $nssSO_4^{2-}$ concentration
281 was lower than in March 2017 (average values of 120 ng/m^3 and 586 ng/m^3 in March 2016 and 2017,
282 respectively). Unfortunately, the sampling stopped in April for technical problems, therefore the HA for the
283 year 2016 can not be completely characterized. Several studies (Overland and Wang, 2016; Cullather et al.,
284 2016) define winter 2015-16 as the warmest winter over the Arctic in the observational record since 1950.
285 Warm anomalies over the central Arctic are associated with physical processes including the presence of
286 enhanced atmospheric water vapor and an increased downwelling longwave radiative flux (Cullater et al.,
287 2016), but atmospheric circulation played a major role in producing such extreme winter 2016 Arctic
288 temperatures. In particular, the splitting of the tropospheric polar vortex over the Arctic occurred in
289 January-March 2016 (Overland and Wang, 2016) and produces a reduced transport of pollutants from
290 continental areas to the Arctic.
291 Figure 3b shows the temporal trend of metals with the largest EF in the aerosol samples collected at Thule:
292 Pb, As, and Cd. These three metals clearly show maximum values in the 2017 AH period, whit other short
293 time concentration spikes. It is interesting to notice that very high concentrations of these metals are
294 measured (1.25 ng/m^3, 0.95 ng/m^3, 0.039 ng/m^3 for Pb, As and Cd, respectively) in late February - March
295 2017, making these metals important tracers for AH and for long distance aerosol transport processes
296 As reported above backward trajectory analysis in late February-March air masses arises mainly by Canada
297 and Nord America and in some days from the North Pole. Polluted air masses located in these areas are the
298 source of Pb, As and Cd. A previous study on aerosol source apportion by positive matrix factorization at
299 Summit Station located on the Greenland ice sheet at 3200 m elevation a.s.l. (Van Curren et al., 2012)

reveals a factors called “arctic haze” characterized by Pb and Mo (other than sulfur). This factor presents a not well defined seasonality, but it is characterized by air masses coming from Arctic Ocean basin and north Canada. In spite of the difference in transport processes and sources impact between the high altitude site (Summit Station) and low elevation station (THAO), arctic haze aerosol reaching the two site have the same source areas.

Ni, V, Cr

These three elements are generally considered anthropogenic markers but, as discussed previously, the data from Thule do not show large values of EFs for these elements. Among the three metals, only V present a significant correlation with Al (R^2 = 0.608) but slope about twice than V/Al in the UCC (Figure 1S). We suggest a crustal source for V but somewhat enriched in V with respect to the mean composition of the crust. By looking at Ni, V and Cr temporal patter, they show no common patterns with nssSO_4^{2-} and do not display significant highest concentration during the AH period. Ni and especially V are commonly used as markers of ship emissions. When this source is dominant, V and Ni display a close linear correlation and the V-to-Ni ratio is comprised between 2.5 and 4.5 (Becagli et al., 2017; Viana et al., 2014). At Thule, V and Ni do not appear to be correlated (figure 4a), and the V-to-Ni ratio is usually lower than that expected from ship emissions, and also lower than $(V/Ni)_{ucc}$ = 2.06 w/w (Handerson and Henderson 2009). This result implies that the aerosol samples at Thule are enriched in Ni with respect to UCC.

It is interesting to note that in some days the V-to-Ni ratio becomes larger than 3, especially in summer. This pattern could be due to sporadic influence from ship aerosols, arising from ships passing through Baffin Bay and arriving in northern Greenland in summer, when sea ice conditions allow navigation. Backward trajectories calculated for summer days characterized by V to Ni ratio larger than 2.5 show that air masses travel at low velocity and low level over Baffin Bay before arriving to Thule (figure 5a). The air masses come from the west-south-west sector and it very unlikely that emissions from the air base located north of the sampling site could be the cause of the increased V-to-Ni ratio. All these evidence (air mass beck trajectories and V to Ni ratio higher than 2.5 in summer period when Baffin bay is ice free) highlight the source from ship passing through Baffin Bay. However, during these events of ship aerosol, V and Ni

concentrations are quite low, suggesting that this source does not greatly affect the concentration of these metals.

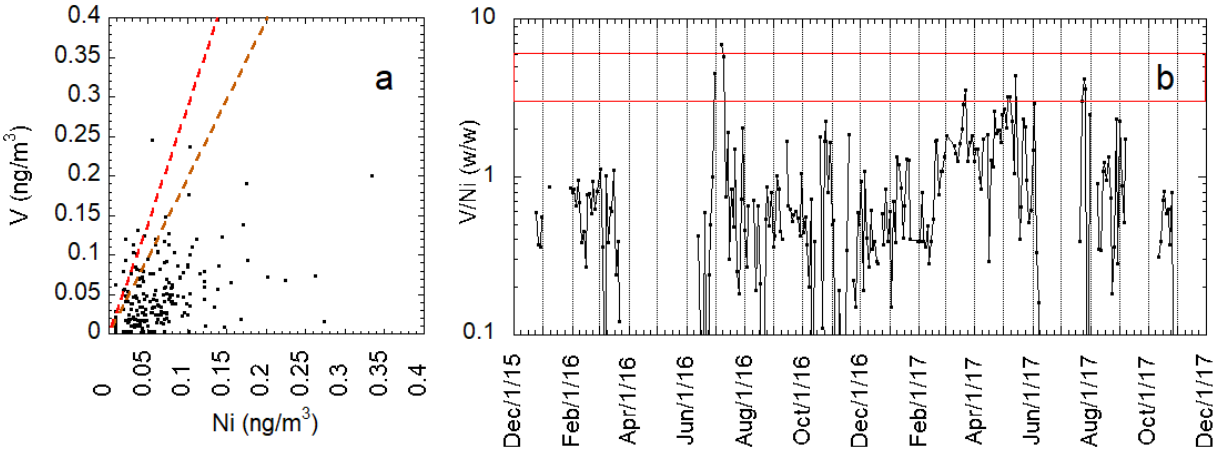

Figure 4. Vanadium – Nickel scatter plot (a). The red dashed line in plot a represents the V-to-Ni ratio characteristic of ship emission (Becagli et al. 2017), and the brown dashed line represents the UCC ratio (Handerson and Henderson, 2009). Plot b shows the temporal evolution of the V-to-Ni ratio in the aerosol samples. Red lines enclose the V/Ni range that could be attributed to ship emissions.

Days showing the highest concentration of Ni (higher than 90° percentile), present V to Ni ratio < 3 and lower than UCC ratio, and also high concentration of Cr.

In general, the aerosol Cr concentrations at Thule are larger than those of Ni and V. The Cr EF is about 10 and shows no evidence of increased concentrations during the AH period. Cr concentrations in the soil are quite variable: average Cr concentration in the earth crust, basalt, shale, and granite is 100, 200, 100 and 20 μg/g, respectively (Krauskopf, 1979). Cr concentration ranges from 1 to 1750 μg/g in rocks from the Skaergaard intrusion in Kangerlussuaq areas (Wager and Mitchell, 1951). Cr and Ni are shown to be associated and strongly concentrated in the early rocks in Greenland (Wager and Mitchell, 1951).

345 Conversely, V (together with P, Cu, Sc, Mn and S) is more related to middle, or late middle, stages
346 represented by certain olivine-free gabbros and ferrogabbros minerals (Wager and Mitchell, 1951).
347 Backward trajectories calculated for days presenting high concentrations of Ni (larger than 2 ng/m^3) and Cr
348 (larger than 0.25 ng/m^3), and consequently a V to Ni ratio lower than UCC, show a clear common pattern
349 with air masses arising from south west Greenland and passing over free of snow areas along the coast line
350 (figure 5b). Therefore, the presence of minerals with high Cr and Ni concentrations in the Greenland soil
351 could explain Cr and Ni concentration levels, EF and mean values of V/Ni lower than UCC in the aerosol
352 sampled at Thule.

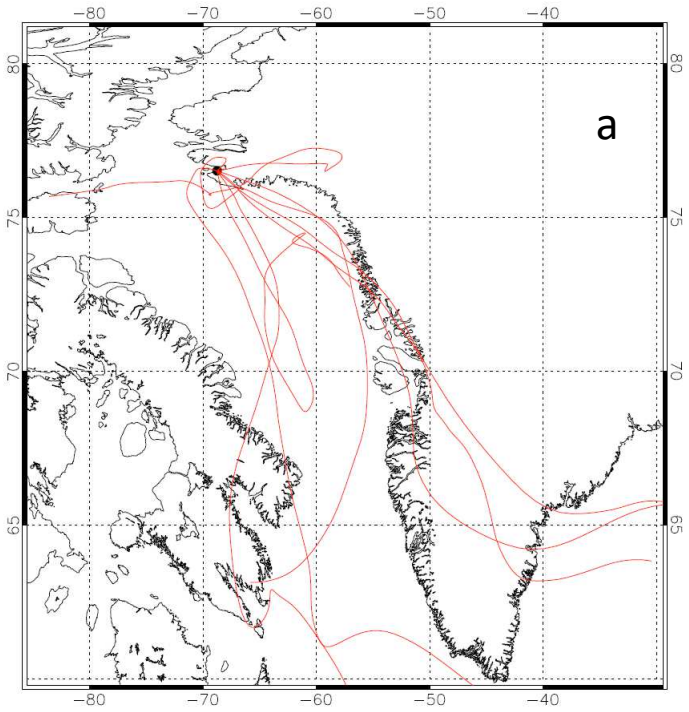

353

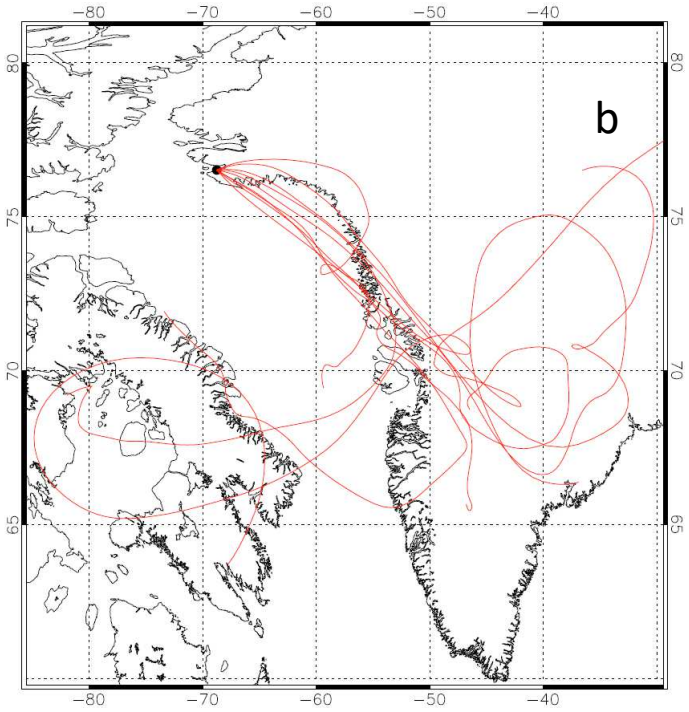

354

355 **Figure 5.** Backward trajectories calculated for days presenting V/Ni > 2.5 (plot a) and for day showing high
356 concentrations of Cr and Ni (larger than 0.25 and 2 ng/m^3, respectively) (plot b) and consequently a V /Ni
357 ratio lower than UCC.

358

359 **La and Ce**

360 In Greenland, there are several large REE deposits in various geological settings (Stensgaard et al., 2016).
361 The largest deposits are in the peralkaline intrusion in south Greenland (near Narsarsuaq). Additionally,
362 four carbonatite-related REE deposits are known from the west coast (Qeqertarsuaq), and one alkaline
363 intrusion (Kap Simpson) and one palaeoplacer deposit (Milne Land) are located in east Greenland (at about
364 200 km north and 200 km west with respect to Ittoqqortoormiit) (Stensgaard et al., 2016).
365 Although La and Ce are the most abundant REEs, they present very low concentrations in the Thule aerosol
366 samples (figure 2a). The percentage of values higher than DL is 90% and 32% for La and Ce, respectively. In
367 spite of the low number of significantly higher than DL values for Ce, some considerations on these two
368 REEs can be made.

Both La and Ce show a significant correlation with Al (R^2 = 0.533 and R^2 = 0.440, respectively figure 1S) demonstrating their common crustal source. Additional information can be derived from the La/Ce ratio time series (figure 4S). Figure 4S shows that La/Ce is usually < 1, but is >1 for samples collected during the AH period and especially in March. La/Ce in the range 1-13 is found in aerosol arising from refineries (Du and Turner 2015) because of the use of La in the zeolitic fluidized-bed catalytic cracking. As previous observed, in March the air masses come from Canada and Nord America where a large number of high refining capacity refinery are present (https://www.oilsandsmagazine.com/projects/canadian-refineries). The La/Ce May is lower than in March but still higher than 1, at this time backward trajectory show that air masses arise from south west Greenland. The REE composition in different Greenland areas may have different percentages of Ce and La. For instance, the REE composition in Tikiusaaq (near Nuuk, South Greenland) is enriched in La (47% Ce, 33% La, 12% Nd, 4% Pr and 4% other REEs) respect to the carbonatite present in Qeqertarsaq (south west Greenland; 50% Ce, 27% La, 16% Nd, 5% Pr and 2% other REEs; Stensgaard et al., 2016). This variability can explain the variability of La/Ce ratio values around the mean values of the UCC (La/Ce =0.5) in months not affected by aerosol from anthropized areas of Canada and North America

4. Summary and conclusions

Metals are powerful markers capable of constraining the different aerosol sources. Data on metals in the Arctic aerosol are however scarce, due to their low concentration in such a matrix. This work reports measurements of metal concentrations and temporal trends of several metals in Arctic aerosols sampled at the Thule High Arctic Atmospheric Observatory (THAAO), in North Western Greenland. Metals are determined in PM_{10} sampled at 48h resolution by an improved easy-to-use high sensitive analytical method ICP-AES (Inductively Coupled Plasma – Atomic Emission Spectroscopy) technique, coupled with a desolvatation inlet system to increase the analytical performance of the technique.

The main results of this work can be summarized as follows:

- Arctic haze at Thule is enriched in Pb, As, and Cd arising from Canada and North America. During the AH period, these metals present concentrations up to 1.25 ng/m^3, 0.95 ng/m^3, 0.039 ng/m^3 for Pb, As and Cd, respectively. These values are one order of magnitude higher than the respective median values. These metals are therefore useful to identify aerosol long-range transport events.

- Metals generally considered as anthropogenic as V, Ni and Cr are here affected mainly by the natural crustal source. The aerosol samples are enriched in V, Ni and Cr with respect to UCC due to the presence of soil enriched in Ni and Cr in southwest Greenland. Backward trajectories confirm the origin of the air masses from the area characterized by soil enriched in these metals. Nevertheless, in a few summer samples the V-to-Ni ratio becomes larger than 3. This pattern is due to a sporadic contribution from ship aerosol coming from ships passing through Baffin Bay and reaching northern Greenland during summer, thanks to the break of sea ice in Baffin Bay and the slow advection of air masses from Baffin Bay towards Thule.

This result is important as we find a clear fingerprint for aerosol coming from Greenland soil (V/Ni < 2) and aerosol from ships (V/Ni>3). The capability to distinguish between the two sources becomes particularly important if the Arctic ship traffic increases as expected.

- Also the typical crustal markers ratios Fe/Al and Ti/Al allow us to distinguish between long-range and local crustal aerosol. In particular, the presence of Ilmenite minerals in the Greenlandic soil, which is enriched in Ti and Fe, allows us to distinguish local sources (Fe/Al=0.89 Ti/Al=0.07) from long-range sources (Fe/Al=0.79 Ti/Al=0.04).

-Finally, the two most abundant REEs (La and Ce) are determined by ICP-AES in 90% and 32% of the samples for La and Ce, respectively. They present a significant correlation with Al, confirming their general common crustal source. Values of La/Ce > 1 are related to anthropogenic aerosol arising from Canada and Nord America enriched in La with respect to natural sources due to the presence of a large number of refineries. Conversely, values of La/Ce < 1 appear to be associated with Greenland soils presenting a different percentage of REEs.

At the present time, the Arctic ecosystem is affected by air pollution coming from the industrialized mid-latitude regions. However, as global warming continues, ship traffic and mining activities could increase, especially in Greenland, and the anthropogenic pressure on this fragile environment would therefore increase. Understanding the processes that control sources and sinks of Arctic air pollutants and their impacts on Arctic communities is therefore crucial. Deficiencies in predictive capabilities and a lack of observations at high latitudes are the major challenges for advancing this understanding and for producing reliable near- and long-term projections of Arctic environmental change.

Acknowledgments: This research was partially funded by the Italian Ministry of University and Research (MIUR) within the framework of the projects Dirigibile Italia: una piattaforma per lo studio multi-disciplinare dei cambiamenti climatici nella regione artica e della loro influenza sulle medie latitudini (PRIN-2007); ARCTICA-ARCTic Research on the Interconnections between Climate and Atmosphere (PRIN 2009); Observations of changes in chemical composition and physical properties of Polar Atmospheres from NDACC Stations (PNRA 2010–2012); ARCA-Arctic: present climatic change and past extreme events (MIUR 2014–2016); SVAAP—The study of the water vapor in the polar atmosphere (PNRA 2015–2016); OASIS-YOPP—Observations of the Arctic Stratosphere In Support of YOPP (PNRA 2016–2018).

The authors gratefully acknowledge the NOAA Air Resources Laboratory (ARL) for the provision of the HYSPLIT transport and dispersion model used in this publication.

References

Aliabadi, A.A. , Staebler, R. M., Sharma, S., 2015. Air quality monitoring in communities of the Canadian Arctic during the high shipping season with a focus on local and marine pollution. Atmos. Chem. Phys., 15, 2651–2673. https://doi.org/10.5194/acp-15-2651-2015.

442 Andrew, R., 2014. Socio-Economic Drivers of Change in the Arctic. AMAP Technical Report No. 9 . Norway:
443 Arctic Monitoring and Assessment Programme (AMAP). http://www.amap.no/documents/doc/Socio-
444 Economic-Drivers-of-Change-in-the-Arctic/1115.
445 Barron, E. J., 1983. *A warm, equable cretaceous: The nature of the problem*. Earth-Sci. Rev. 19, 305–338.
446 Barrie, L.A., G. Hartog, J. Bottenheim, and S. Landsberger, 1989. Anthropogenic aerosols and gases in the
447 lower troposphere at Alert, Canada in April, 1986. J. Atmos. Chem., 9, 101-128.
448 Becagli, S., Anello, F., Bommarito, C., Cassola, F., Calzolai, G., Di Iorio, T., di Sarra, A., Gómez-Amo, J.-L.,
449 Lucarelli, F., Marconi, M., Meloni, D., Monteleone, F., Nava, S., Pace, G., Severi, M., Sferlazzo, D. M.,
450 Traversi, R., Udisti, R., 2017. Constraining the ship contribution to the aerosol of the central
451 Mediterranean Atmos. Chem. Phys., 17, 2067–2084. www.atmos-chem-
452 phys.net/17/2067/2017/doi:10.5194/acp-17-2067-2017.
453 Becagli, S., Lazzara, L., Marchese, C., Dayan, U., Ascanius, S.E., Cacciani, M., Caiazzo, L., Di Biagio, C., Di Iorio,
454 T., di Sarra, A., Eriksen, P., Fani, F., Giardi, F., Meloni, D., Muscari, G., Pace, G., Severi, M., Traversi, R.,
455 Udisti, R., 2016. Relationships linking primary production, sea ice melting, and biogenic aerosol in the
456 Arctic. Atmos. Environ, 136, 1-15. http://dx.doi.org/10.1016/j.atmosenv.2016.04.002.
457 Bekryaev, R. V., Polyakov, I. V., Alexeev, V. A., 2010. Role of polar amplification in long-term surface air
458 temperature variations and modern arctic warming. J. Clim. 23, 3888–3906.
459 Chapman, W. L., Walsh, J. E., 1993. Recent variations of sea ice and air temperature in high latitudes. Bull.
460 Am. Meteorol. Soc. 74, 33–47.
461 Conca, E., Abollino, O., Giacomino, A., Buoso, S., Traversi, R., Becagli, S., Grotti, M., Malandrino, M., 2019.
462 Source identification and temporal evolution of trace elements in PM10 collected near to Ny-Ålesund
463 (Norwegian Arctic). Atmos. Environ. 203, 153–165, 2019.
464 https://doi.org/10.1016/j.atmosenv.2019.02.001.
465 Corbett, J.J., Lack, D.A., Winebrake, J.J., Harder, S., Silberman, J.A., Gold, M., 2010. Arctic shipping emissions
466 inventories and future scenarios. Atmos. Chem. Phys. 10, 9689–9704. DOI: 10.5194/acp-10-9689-2010.

467 Cullather, R. I., Lim Y.-K., Boisvert L. N., Brucker L., Lee J. N., Nowicki S. M. J., 2016. Analysis of the warmest
468 Arctic winter, 2015–2016. Geophys. Res. Lett., 43, 10,808–10,816. DOI:10.1002/2016GL071228.
469 Dahl-Jensen, D., Mosegaard, K., Gundestrup, N., Clow G. D., Johnsen, S. J., Hansen, A. W., Balling, N., 1998.
470 Past temperatures directly from the Greenland ice sheet. Science 282, 268–271. DOI:
471 10.1126/science.282.5387.268.
472 Du, L. and Turner, J., 2015. Using PM2.5 lanthanoid elements and nonparametric wind regression to track
473 petroleum refinery FCC emissions. Sci. Total. Environ., 529, 65–71. doi:10.1016/j.scitotenv.2015.05.034.
474 Eckhardt, S., Hermansen, O., Grythe, H., Fiebig, M., Stebel, K., Cassiani, M., Baecklund, A., Stohl, A., 2013.
475 The influence of cruise ship emissions on air pollution in Svalbard—A harbinger of a more polluted
476 Arctic?. Atmos. Chem. and Phys., 13, 8401–8409. DOI: 10.5194/acp-13-8401-2013.
477 Gautier, D. L., Bird, K. J., Charpentier, R. R., Grantz, A., House-knecht, D. W., Klett, T. R., Moore, T. E.,
478 Pitman, J. K., Schenk,C. J., Schuenemeyer, J. H., Sørensen, K., Tennyson, M. E., Valin,Z. C., and Wandrey,
479 C. J. , 2009. Assessment of Undiscovered Oil and Gas in the Arctic. Science, 324, 1175–1179.
480 Giardi, F., Traversi, R., Becagli, S., Severi, M., Caiazzo, L., Ancillotti, C., Udisti, R., 2018. Determination of
481 Rare Earth Elements in multi-year high-resolution Arctic aerosol record by double focusing Inductively
482 Coupled Plasma Mass Spectrometry with desolvation nebulizer inlet system. Sci. of the Total Environ.
483 613–614, 1284–1294. https://doi.org/10.1016/j.scitotenv.2017.09.247.
484 Gong S.L., Barrie, L.A., 2005. Trends of heavy metal components in the Arctic aerosols and their relationship
485 to th, emissions in the Northern Hemisphere. Science of the Total Environment, 342, 175– 183.
486 Henderson, P. and Henderson, G. M., 2009.The Cambridge Handbook of Earth Science Data, Cambridge,
487 University Press, Cambridge, 42–44.
488 Henriksen, N., Higgins, A.K., Kalsbeek, F., Pulvertaft, T.C.R., 2009. Greenland from Archaean to Quaternary.
489 Descriptive text to the 1995 Geological map of Greenland, 1:2 500 000. 2nd edition. Geological Survey of
490 Denmark and Greenland Bulletin 18, 126 pp. + map.
491 Holland, M., Bitz, C. 2003. Polar amplification of climate change in coupled models. Clim. Dynam. 21, 221–
492 232.

493 Krauskopf, K.B., 1979. Introduction to Geochemistry. McGraw Hill, New York.
494 Law, K.S., Roiger, A., Thomas, J. L., Marelle, L., Raut, J.-C., Dalsøren, S., Fuglestvedt, J., Tuccella, P.,
495 Weinzierl, B., Schlager H., 2017. Local Arctic air pollution: Sources and impacts. Ambio., 46, 453–463.
496 doi: 10.1007/s13280-017-0962-2.
497 Muscari, G., Di Biagio, C., di Sarra, A., Cacciani, M., Ascanius, S.E., Bertagnolio, P.P., Cesaroni, C., de Zafra,
498 R.L., Eriksen, P., Fiocco, G., Fiorucci, I., Fua, D., 2014. Observations of surface radiation and stratospheric
499 processes at Thule Air Base, Greenland, during the IPY. Ann. Geophys. 57 (SS0323), 1-14.
500 Overland, J. E., and Wang, M., 2016. Recent extreme Arctic temperatures are due to a split polar vortex. J.
501 Clim., 29(15), 5609–5616. DOI:10.1175/JCLI-D-16-0320.1.
502 Peters, G., Nilssen, T., Lindholt, L., Eide, M., Glomsrød, S., Eide, L. I., Fuglestvedt, J. S., 2011. Future
503 emissions from shipping and petroleum activities in the Arctic. Atmos. Chem. Phys. 11, 5305–5320. DOI:
504 10.5194/acp-11-5305-2011.
505 Peters, G.P., Nilssen, T.B., Lindholt, L., Eide, M.S., Glomsrød, S., Eide, L.I., Fuglestvedt, J.S., 2011. Future
506 emissions from shipping and petroleum activities in the Arctic. Atmos. Chem. and Phys., 11, 5305–5320.
507 DOI: 10.5194/acp-11-5305-2011.
508 Pithan, F., Mauritsen, T., 2014. Arctic amplification dominated by temperature feedbacks in contemporary
509 climate models. Nature Geoscience, 7, 181-184. DOI: 10.1038/NGEO2071.
510 Quinn, P. K., Shaw, G., Andrews, E., Dutton, E. G., Ruoho-Airola, T., Gong, S. L., 2007. Arctic haze: Current
511 trends and knowledge gaps. Tellus, 59B, 99–114.
512 Rugi, F., Udisti. R., Becagli, S., Frosini, D., Giorgetti, G., Kuhn, G., Marconi, M., Monien, D., Nava, S., Severi,
513 M., Talarico, F., Traversi R., 2015. One-million year Rare Earth Element stratigraphies along an Antarctic
514 marine sediment core. Microchemical Journal 122, 164–171.
515 Shaw, G.E., 1995. The Arctic Haze Phenomenon, 1995. Bulletin of the American Meteorological Society, 76
516 (12), 2403-2414.
517 Shevchenko, V., Lisitzin, A., Vinogradova, A., Stein R., 2003. Heavy metals in aerosols over the seas of the
518 Russian Arctic. Sci. of the Tot. Environ. 306, 11–25.

519 Stensgaard, B. M., Stendal, H., Kalvig P., Hanghøj K., 2016. Review of potential resources for critical
520 minerals in Greenland. MiMa report 2016/3, 72 pages.
521 Stein, A.F., Draxler, R.R, Rolph, G.D., Stunder, B.J.B., Cohen, M.D., and Ngan, F., 2015. NOAA's HYSPLIT
522 atmospheric transport and dispersion modeling system, Bull. Amer. Meteor. Soc., 96, 2059-2077,
523 http://dx.doi.org/10.1175/BAMS-D-14-00110.1
524 Stohl, A., Klimont, Z., Eckhardt, S., Kupiainen, K., Shevchenko, V., Kopeikin, V., Novigatsky, A. 2013. Black
525 carbon in the Arctic: The underestimated role of gas flaring and residential combustion emissions.
526 Atmos. Chem. Phys. 13, 8833– 8855. DOI: 10.5194/acp-13-8833-2013.
527 VanCurren, R.A., Cahil, T., Burkhart, J., Bernes D., Zhao, Y., Perry, K., Cliff, S., McConnell, J., 2012. Aerosols
528 and their sources at Summit Greenland – First results of continuous size- and time-resolved sampling.
529 Atmos. Environ. 52, 82-97.
530 Viana, M., Hammingh, P., Colette, A., Querol, X., Degraeuwe, B., de Vlieger, I., and van Aardenne, J., 2014.
531 Impact of maritime transport emissions on coastal air quality in Europe. Atmos. Environ., 90, 96–105.
532 Wager, L.R., Mitchell, R.L., 1951.The distribution of trace elements during strong fractionation of basic
533 magma - a further study of the Skaergaard intrusion, East Greenland. Geochimica et Cosmochimica Acta,
534 1(3), 129-208. https://doi.org/10.1016/0016-7037(51)90016-6.
535 Zhan J., Gao Y., Li W., Chen L., Lin H., Lin Q., 2014. Effects of ship emissions on summertime aerosols at Ny–
536 Alesund in the Arctic. Atmospheric Pollution Research, 5, 500-510. doi:10.5094/APR.2014.059.

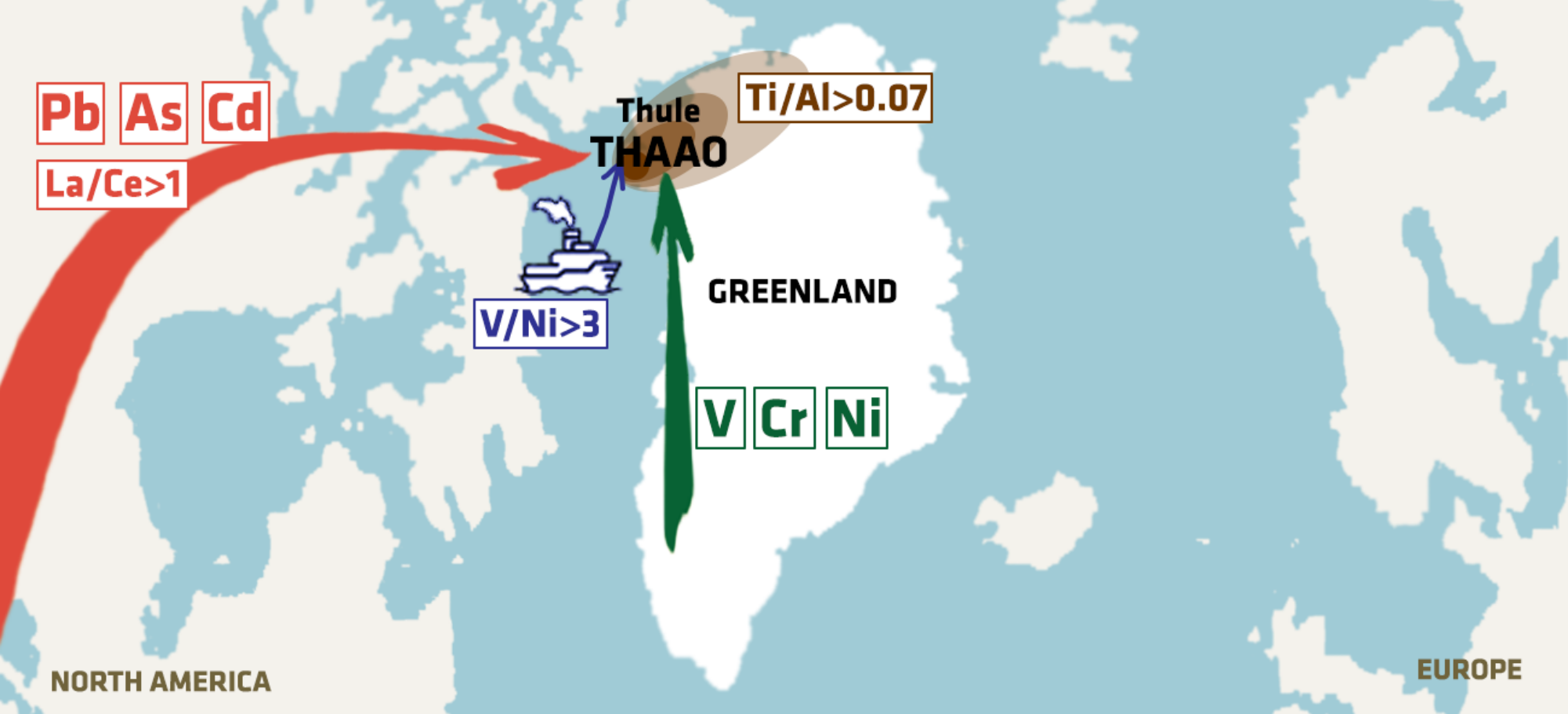
Pb
As
Cd
La/Ce>1
Thule
THAAO
Ti/Al>0.07
V/Ni>3
GREENLAND
V
Cr
Ni
NORTH AMERICA
EUROPE